10-2018

iac Gene Expression in the Indole-3-Acetic Acid-Degrading Soil Bacterium *Enterobacter soli* LF7

Isaac V. Greenhut
University of Kentucky, ivgreenhut@uky.edu

Beryl L. Slezak
University of California - Davis

Johan H. J. Leveau
University of California - Davis

Right click to open a feedback form in a new tab to let us know how this document benefits you.

Follow this and additional works at: https://uknowledge.uky.edu/pss_facpub

Part of the Bacteria Commons, Genetics and Genomics Commons, Microbiology Commons, Plant Sciences Commons, and the Soil Science Commons

Repository Citation

iac **Gene Expression in the Indole-3-Acetic Acid-Degrading Soil Bacterium** *Enterobacter soli* **LF7**

AMERICAN SOCIETY FOR MICROBIOLOGY | **Applied and Environmental Microbiology**®

iac Gene Expression in the Indole-3-Acetic Acid-Degrading Soil Bacterium *Enterobacter soli* LF7

Isaac V. Greenhut,ª* Beryl L. Slezak,ª* Johan H. J. Leveauª

ªDepartment of Plant Pathology, University of California, Davis, California, USA

ABSTRACT We show for soil bacterium *Enterobacter soli* LF7 that the possession of an indole-3-acetic acid catabolic (*iac*) gene cluster is causatively linked to the ability to utilize the plant hormone indole-3-acetic acid (IAA) as a carbon and energy source. Genome-wide transcriptional profiling by mRNA sequencing revealed that these *iac* genes, chromosomally arranged as *iacHABICDEFG* and coding for the transformation of IAA to catechol, were the most highly induced (>29-fold) among the relatively few (<1%) differentially expressed genes in response to IAA. Also highly induced and immediately downstream of the *iac* cluster were genes for a major facilitator superfamily protein (*mfs*) and enzymes of the β-ketoadipate pathway (*pcaIJD-catBCA*), which channels catechol into central metabolism. This entire *iacHABICDEFG-mfs-pcaIJD-catBCA* gene set was constitutively expressed in an *iacR* deletion mutant, confirming the role of *iacR*, annotated as coding for a MarR-type regulator and located upstream of *iacH*, as a repressor of *iac* gene expression. In *E. soli* LF7 carrying the DNA region upstream of *iacH* fused to a promoterless *gfp* gene, green fluorescence accumulated in response to IAA at concentrations as low as 1.6 μM. The *iacH* promoter region also responded to chlorinated IAA, but not other aromatics tested, indicating a narrow substrate specificity. In an *iacR* deletion mutant, *gfp* expression from the *iacH* promoter region was constitutive, consistent with the predicted role of *iacR* as a repressor. A deletion analysis revealed putative −35/−10 promoter sequences upstream of *iacH*, as well as a possible binding site for the IacR repressor.

IMPORTANCE Bacterial *iac* genes code for the enzymatic conversion of the plant hormone indole-3-acetic acid (IAA) to catechol. Here, we demonstrate that the *iac* genes of soil bacterium *Enterobacter soli* LF7 enable growth on IAA by coarrangement and coexpression with a set of *pca* and *cat* genes that code for complete conversion of catechol to central metabolites. This work contributes in a number of novel and significant ways to our understanding of *iac* gene biology in bacteria from (non-)plant environments. More specifically, we show that LF7's response to IAA involves derepression of the MarR-type transcriptional regulator IacR, which is quite fast (less than 25 min upon IAA exposure), highly specific (only in response to IAA and chlorinated IAA, and with few genes other than *iac*, *cat*, and *pca* induced), relatively sensitive (low micromolar range), and seemingly tailored to exploit IAA as a source of carbon and energy.

KEYWORDS *Enterobacter asburiae* LF7a, *Enterobacter soli* LF7, IAA, auxin, *iac* genes, indole-3-acetic acid catabolism

Address correspondence to Johan H. J. Leveau, jleveau@ucdavis.edu.

* Present address: Isaac V. Greenhut, Department of Plant and Soil Sciences, University of Kentucky, Lexington, Kentucky, USA; Beryl L. Slezak, Illumina, San Diego, California, USA.

The ability of bacteria to degrade the plant hormone indole-3-acetic acid (IAA) has been recognized for over 60 years (1), but it was not until more recently (2) that a set of genes underlying this property was first described and characterized. These so-called *iac* genes have since been identified in the genomes of representatives from the bacterial classes *Alphaproteobacteria*, *Betaproteobacteria*, and *Gammaproteobacteria* as well as the phylum *Actinobacteria* (2). Many *iac*-carrying species are known to

associate with plants, but some are not, which has raised questions about the ecological role(s) of *iac* genes (2).

Pseudomonas putida 1290 was the strain for which a link between *iac* genes and IAA catabolism was first demonstrated (2). Originally isolated from the foliage of a pear tree, *P. putida* 1290 can use IAA as a sole source of carbon, nitrogen, and energy (3). It carries the *iac* genes clustered on the chromosome as *iacABCDEFG*→-*iacR*←-*iacHI*→ (superscript arrows indicate the relative orientation of single genes or groups of genes). This cluster was sufficient to confer upon *P. putida* KT2440 (not an *iac* gene carrier) the ability to grow on IAA (2). Heterologous expression of the *iac* gene cluster in *Escherichia coli* revealed that *iacA* is involved in the initial conversion of IAA to 2-hydroxy-IAA (2-OH-IAA), which is then converted via 3-hydroxy-2-oxo-IAA (diOxIAA) to catechol, the end product of the *iac*-encoded IAA degradation pathway (4). In *P. putida* 1290, catechol is *ortho* cleaved and channeled into central metabolism by-products of the *cat* and *pca* genes (2). These *cat* and *pca* genes are necessary for the growth of *P. putida* 1290 on IAA as the sole source of carbon and energy (2).

Two other bacterial strains for which *iac* gene function has been confirmed are *Acinetobacter baumannii* ATCC 19606 and *Paraburkholderia phytofirmans* PsJN. The first of these two strains was isolated from a patient with a urinary tract infection and carries its *iac* genes as *iacR*←-*iacHABICDEFG*→ (5). Wild-type *Acinetobacter baumannii* ATCC 19606, but not the *iacA*-inactivated transposon mutant AB6-2, was able to grow on M9 minimal medium with IAA as a sole carbon source, while crude cell extracts of ATCC 19606 but not mutant AB6-2 showed IAA catabolic activity (6). Both sets of observations confirm a role for IacA in the IAA degradation pathway. The ability to grow on IAA was also demonstrated for the *iac*-carrying plant-growth-promoting rhizobacterium *P. phytofirmans* PsJN (7). In this strain, originally isolated from onion roots, the organization of *iac* genes is more complex than in strains 1290 and ATCC 19606 (*iacF*→-*catCAB*←-*catR1*→-*iacR2*←-*iacCDYT1*→-*iacS*←-*iacABIHE*→-*iacR1*←-*iacG*→, with a second locus *iacT2*→-*iacA2G2*→ elsewhere on the chromosome), with *iac* genes separated into what appear to be multiple transcriptional units, sometimes present in more than one copy (e.g., *iacA*), and interspersed with *cat* and other nonarchetypal *iac* genes (e.g., *iacY*). In strain PsJN, insertional inactivation of *iacA1*, *iacB*, *iacC*, *iacD*, *iacE*, *iacF*, *iacH*, or *iacI*, but not *iacA2*, *iacG*, *iacG2*, *iacY*, *iacS*, *iacT1*, or *iacT2*, led to a loss of the ability to grow on IAA, thus conclusively linking *iacF*, *iacCD*, and *iacABIHE* to the IAA degradative phenotype (7).

The regulation of *iac* gene expression has been studied in all three strains for which *iac* genes have been linked to IAA degradation. Reverse transcription quantitative PCR (RT-qPCR) showed that the expression of *iac* genes in *P. putida* 1290 and *P. phytofirmans* PsJN was inducible with IAA (4, 7). Similarly, the exposure to IAA led to the production of IacA protein in *A. baumannii* ATCC 19606 (5, 6). In the case of *P. putida* 1290 and *A. baumannii* ATCC 19606, experimental evidence suggests a role for the *iacR* gene product in *iac* gene expression. A derivative of the *P. putida* 1290 *iac* gene cluster with the *iacR* gene insertionally inactivated (i.e., *iacABCDEFG*-*iacR*::Tn5-*iacHI*) showed constitutive *iac* expression in heterologous host *E. coli* (4), suggesting that *iacR* codes for a repressor of *iac* genes in *P. putida* 1290. As for *A. baumannii* ATCC 19606, the use of an *E. coli* reporter system consisting of an isopropyl β-D-1-thiogalactopyranoside (IPTG)-inducible *iacR* gene and the *iacH* promoter fused to the gene for green fluorescent protein (*gfp*), revealed that the induction of *iacR* diminished GFP production, suggesting that the product of *iacR* represses *iac* gene expression. Furthermore, in electrophoretic mobility shift assays, purified IacR from ATCC 19606 was shown to bind to a DNA fragment encompassing the *iacR*-*iacH* intergenic region in the absence of IAA and to lose the affinity for this region in the presence of IAA (6). These findings are consistent with the annotation of *iacR* as coding for a MarR, or multiple antibiotic resistance repressor, family-type protein and with a model of *iac* gene expression that involves IAA as an inducer of its own degradation in *P. putida* 1290 and *A. baumannii* ATCC 19606. Unlike the *iacR* gene products in these two strains, *iacR1* and *iacR2* from *P. phytofirmans* PsJN are predicted transcriptional regulators of the LuxR and LysR families,
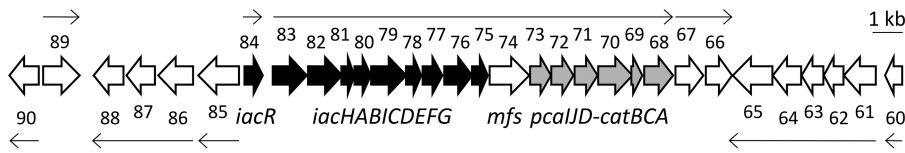
FIG 1 Graphical representation of the region of the *E. soli* LF7 chromosome (CP003026) which harbors the *iacR-iacHABICDEFG* gene cluster. Individual genes are represented as block arrows, and shown for each gene are its relative size, direction, and location, as well as the last two digits of its NCBI locus_tag Entas_24xx (e.g., for *iacH*, xx equals 83 because its locus tag is Entas_2483). Highlighted in black are the *iac* genes, in gray are the *pcaIJD* and *catBCA* genes. Line arrows indicate the size and direction of transcriptional units (operons) as predicted by FGENESB.

respectively. It was proposed that the regulation of *iac* gene expression in PsJN involves the product of *iacS*, which is a sensor kinase that stimulates IacR1 upon recognition of IAA, which in turn activates the expression of *iacABIHE* and *iacG*. This transcriptional activation then initiates the IAA degradation pathway and leads to the accumulation of diOxIAA, which, together with IacR2, acts to induce the expression of *iacCD* and *iacF* for further conversion into catechol (7).

The organization of *iac* genes into multiple and differently regulated transcriptional units, as appears to be the case for *P. phytofirmans* PsJN, may represent an adaptation that enables bacteria to express only a subset of the IAA degradation pathway components (7). Perhaps for PsJN, which colonizes plants as an endophyte, the possession of *iac* genes gives the bacterium control over its host's IAA homeostasis through IAA inactivation, for which it would be sufficient to express only the first step(s) of the pathway. In bacteria that instead use the *iac* genes to extract carbon and energy from IAA, one would expect the *iac* genes to be more tightly organized, possibly into a single operon, under the control of a single promoter. We identified *Enterobacter soli* LF7 (synonym, *Enterobacter asburiae* LF7a) as a bacterial strain that appears to meet these criteria. Originally isolated from soil in the Tambopata National Reserve (Peru) for its ability to grow on lignin cellulose as a sole source of carbon (8), this bacterium carries the *iac* genes as a contiguous cluster *iacHABICDEFG* with an *iacR* homolog upstream of *iacH* and with *pcaIJD* and *catBCA* genes immediately downstream of, and in the same transcriptional orientation as, *iacG*. We are interested in *E. soli* LF7 as a model strain representing what is arguably the most efficient way to organize *iac* genes on a bacterial genome, i.e., *iac* genes clustered all together, seemingly organized as an operon and syntenically coupled to genes (*cat* and *pca*) that shuttle the product of the *iac*-encoded IAA degradation pathway (catechol) into central metabolism. Here, we report on the coexpression of *iac*, *cat*, and *pca* genes in *E. soli* LF7, the specificity, sensitivity, and speed of *iac* gene induction, and the role of *iacR* as a repressor of *iac* gene expression, as well as the numbers, types, and functions of other genes whose expression is altered in response to IAA.

RESULTS

Organization of the *iac* genes on the LF7 genome and their contribution to the IAA degradative phenotype. The genome of *E. soli* LF7 harbors a complete set of *iac* genes, arranged as *iacR*→-*iacHABICDEFG*→ (Fig. 1). All nine genes immediately downstream of *iacG* have the same orientation as the *iac* genes. These downstream genes include *mfs* (predicted to code for a major facilitator superfamily protein), *pcaIJD* (coding for the conversion of β-ketoadipate enol-lactone to β-ketoadipyl-CoA), *catBCA* (catechol to β-ketoadipate enol-lactone), a gene coding for a fatty acid desaturase (locus Entas_2467), and one for the periplasmic component of an ABC-type transport system (Entas_2466). While there is a 333-bp gap between the stop codon of *iacR* and the start codon of *iacH*, all 17 genes downstream of *iacH* show little or no intergenic space (Fig. 1). An FGENESB analysis predicted an operonic structure for the 16 contiguous genes *iacHABICDEFG-mfs-pcaIJD-catBCA*, while *iacR* and Entas_2467-2466 each constitute a separate single transcriptional unit (Fig. 1).
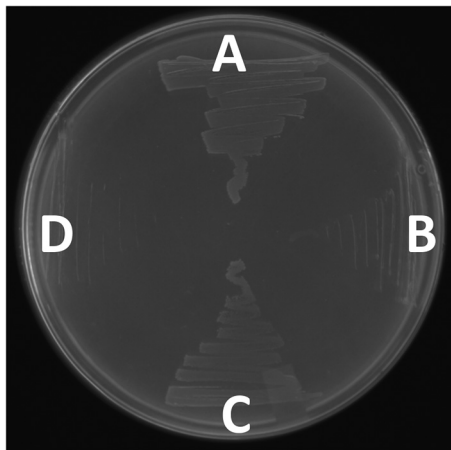
FIG 2 Wild-type *E. soli* LF7 (A), *E. soli* LF7 Δ*iacA::cat* (B), *E. soli* LF7 Δ*iacR::cat* (C), and negative control *E. coli* TOP10 (D) streaked on M9 minimal agar containing 5 mM IAA as the sole source of carbon and energy.

We confirmed that *E. soli* LF7 is able to utilize IAA as a sole source of carbon and energy (Fig. 2A). An *iacA* deletion derivative of *E. soli* LF7 (Δ*iacA::cat*) was not able to grow at the expense of IAA (Fig. 2B), supporting the expected contribution of *iacA* to the IAA-degradative phenotype. An *iacR* deletion mutant of *E. soli* LF7 (Δ*iacR::cat*) was still able to grow on IAA (Fig. 2C), which is consistent with its predicted role as a repressor of *iac* gene expression.

Genome-wide transcriptional profiling of wild-type *E. soli* LF7 and its *iacR* deletion mutant in response to IAA. We collected and compared transcriptome sequencing (RNA-Seq) data from replicate cultures ($n = 3$) of wild-type *E. soli* LF7 (wt) or its Δ*iacR::cat* derivative (mut) which were exposed to 200 μM IAA or water (control) for 2 h while growing exponentially on minimal medium with succinate. We refer to these four treatments as wt+IAA, wt−IAA, mut+IAA, and mut−IAA, respectively. We identified 96 genes (2.1% of the 4,582 genes on the LF7 genome) that were differentially expressed in at least one of the following pairwise comparisons: wt+IAA versus wt−IAA, mut−IAA versus wt−IAA, mut+IAA versus mut−IAA, and mut+IAA versus wt+IAA (Table 1). For each comparison, a gene was considered "differentially expressed" if its calculated value for $\log_2$-fold change (LFC) was greater than 1 or smaller than −1 (i.e., transcript levels were >2-fold higher or lower in one treatment than in the other), with an adjusted *P* value of <0.05. We will describe these differentially expressed genes in more detail below.

The wt+IAA versus wt−IAA comparison revealed 44 differentially expressed genes. Of these, 37 were "induced" in response to IAA (i.e., showed LFC values greater than 1 in wt+IAA compared to that in wt−IAA), while 7 were "repressed" by IAA (Table 1). The 16 highest expressed genes in response to IAA (LFC values of 4.87 to 5.95) were the 16 genes belonging to the *iacHABICDEFG-mfs-pcaIJD-catBCA* cluster (Fig. 3A). This observation is consistent with the observed inducibility of *iac* genes in other bacterial species and with the prediction that in LF7, these genes form a single operonic unit. Also induced were the Entas_2467 fatty acid desaturase gene downstream of *catA* (LFC = 1.9) and the Entas_2485 gene upstream of *iacR* (LFC = 2.13), which is predicted to code for a 4-hydroxyphenylacetate transporter (Fig. 3). The *iacR* gene itself (Entas_2484) was not differentially expressed in response to IAA. Other genes induced by IAA (Table 1) were *mdcABCD* (Entas_4061-4058; LFC = 1.2 to 1.6), annotated as components of the malonate decarboxylase system, as well as genes predicted to code for transcriptional regulators (Entas_2134, _2135), major facilitator superfamily proteins (Entas_0990, _1586, _3302), a homoserine/threonine efflux pump (Entas_4256), a carboxylate/amino acid/amine transporter (Entas_2754), glyoxylate/hydroxypyruvate reductase (Entas_0190), a methyl-accepting chemotaxis protein (Entas_3754), or hypothetical proteins (Entas_1356,

TABLE 1 Differentially expressed genes in wild-type *E. soli* LF7 and its Δ*iacR* deletion mutant exposed (or not) to IAA[a]

Feature	Annotation	wt[b]+IAA vs wt−IAA		mut[c]−IAA vs wt−IAA		mut+IAA vs mut−IAA		mut+IAA vs wt+IAA	
		LFC	P value	LFC	P value	LFC	P value	LFC	P value
Entas_0010	Small heat shock protein			1.73	2.53E−04			1.46	5.93E−04
Entas_0190	Glyoxylate/hydroxypyruvate reductase	1.43	9.58E−07						
Entas_0262	ABC transporter-like protein							−1.20	5.71E−05
Entas_0263	Maltoporin							−1.38	4.59E−04
Entas_0264	Maltose operon, periplasmic							−1.21	6.53E−04
Entas_0268	Hypothetical protein			1.20	1.59E−02				
Entas_0291	Hypothetical protein			−1.06	6.24E−04				
Entas_0470	Aspartate carbamoyltransferase regulatory chain							−1.15	9.53E−03
Entas_0471	Aspartate carbamoyltransferase							−1.19	7.11E−03
Entas_0478	Ornithine carbamoyltransferase							−1.01	5.98E−03
Entas_0511	Amino acid-binding protein			1.36	2.58E−02				
Entas_0525	Carbon starvation protein CstA					2.03	2.15E−06	2.38	6.91E−08
Entas_0539	Hypothetical protein			1.37	3.41E−03				
Entas_0569	LuxR family transcriptional regulator			1.06	3.46E−03				
Entas_0640	Carbamoyl-phosphate synthase, large subunit							−1.03	6.96E−03
Entas_0865	ABC transporter, periplasmic binding protein							1.45	3.64E−02
Entas_0866	ABC transporter-like protein			1.60	3.03E−02				
Entas_0990	Major facilitator superfamily protein	1.84	1.21E−06			1.48	5.53E−05		
Entas_1022	Pili assembly chaperone							−1.08	5.84E−04
Entas_1024	Mannose binding protein FimH							−1.02	6.39E−04
Entas_1079	Hypothetical protein			1.19	3.05E−03				
Entas_1080	Hypothetical protein			1.03	1.06E−02				
Entas_1185	Orn/lys/arg decarboxylase major subunit			1.05	4.08E−03				
Entas_1348	Cationic amino acid ABC transporter periplasmic binding							−1.01	9.01E−04
Entas_1356	Hypothetical protein	1.02	2.90E−03						
Entas_1576	Curlin associated repeat-containing protein			1.28	1.14E−02				
Entas_1586	Major facilitator superfamily protein	1.73	7.84E−06						
Entas_1649	Acyltransferase			1.19	4.33E−02				
Entas_1713	Acetylornithine/succinyldiaminopimelate aminotransferase							1.27	1.94E−03
Entas_1714	Arginine *N*-succinyltransferase							1.08	1.29E−03
Entas_1715	*N*-Succinylglutamate 5-semialdehyde dehydrogenase							1.20	2.08E−03
Entas_1716	*N*-Succinylarginine dihydrolase							1.05	9.85E−04
Entas_1717	Succinylglutamate desuccinylase							1.13	2.03E−03
Entas_1902	Major facilitator superfamily protein					1.03	4.18E−04	1.13	9.49E−05
Entas_1929	Hypothetical protein					−1.09	4.30E−02		
Entas_2047	Diguanylate phosphodiesterase			1.79	8.61E−03				
Entas_2120	Hypothetical protein	1.15	1.73E−02						
Entas_2124	Methionine synthase, vitamin-B12 independent	2.01	1.60E−10			1.33	2.28E−07		
Entas_2134	AraC family transcriptional regulator	1.05	1.93E−04						
Entas_2135	MarR family transcriptional regulator	1.01	2.38E−03						
Entas_2267	Auxin efflux carrier			2.85	1.42E−02				
Entas_2387	OmpW family protein							−1.15	2.38E−02
Entas_2467	Fatty acid desaturase	1.86	8.48E−07	3.32	3.42E−10			2.30	1.24E−08
Entas_2468 (*catA*)	Catechol 1,2-dioxygenase	5.49	4.82E−12	7.21	1.28E−13			2.11	6.91E−08
Entas_2469 (*catC*)	Muconolactone delta-isomerase	5.47	2.71E−10	7.28	5.85E−12			2.37	4.36E−07
Entas_2470 (*catB*)	Muconate and chloromuconate cycloisomerase	5.51	8.18E−12	7.45	1.28E−13			2.60	1.17E−08
Entas_2471 (*pcaD*)	3-Oxoadipate enol-lactonase	5.55	3.90E−12	7.54	5.07E−14			2.58	2.14E−09
Entas_2472 (*pcaJ*)	3-Oxoacid CoA-transferase, subunit B	5.48	4.49E−12	7.53	5.6E−14			2.57	5.20E−09
Entas_2473 (*pcaI*)	3-Oxoacid CoA-transferase, subunit A	5.60	4.49E−12	7.64	6.45E−14			2.58	6.10E−09
Entas_2474 (*mfs*)	Major facilitator superfamily protein	5.32	1.59E−10	7.37	2.40E−12			2.71	6.91E−08
Entas_2475 (*iacG*)	Flavin reductase domain-containing protein FMN-binding protein	5.60	3.36E−10	7.74	5.34E−12			2.77	1.44E−07
Entas_2476 (*iacF*)	Ferredoxin	5.80	1.97E−11	7.92	3.31E−13			2.73	2.72E−08
Entas_2477 (*iacE*)	Short-chain dehydrogenase/reductase	5.70	8.59E−12	7.88	1.28E−13			2.73	1.24E−08
Entas_2478 (*iacD*)	Aromatic-ring-hydroxylating dioxygenase beta subunit	5.95	8.18E−12	8.08	1.28E−13			2.70	1.28E−08
Entas_2479 (*iacC*)	Rieske (2Fe-2S) iron-sulfur domain-containing protein	5.75	4.49E−12	7.90	5.68E−14			2.73	6.97E−09
Entas_2480 (*iacI*)	Hypothetical protein	5.88	8.18E−12	7.99	1.28E−13			2.71	1.24E−08
Entas_2481 (*iacB*)	Hypothetical protein	5.79	3.02E−11	7.84	5.76E−13			2.63	6.77E−08
Entas_2482 (*iacA*)	Acyl-CoA dehydrogenase type protein	5.32	2.03E−08	7.44	3.12E−10			2.90	4.64E−06

(Continued on next page)

TABLE 1 (Continued)

Feature	Annotation	wt[b]+IAA vs wt−IAA		mut[c]−IAA vs wt−IAA		mut+IAA vs mut−IAA		mut+IAA vs wt+IAA	
		LFC	P value	LFC	P value	LFC	P value	LFC	P value
Entas_2483 (iacH)	Amidase	4.87	1.75E−08	6.78	2.71E−10			2.71	4.05E−06
Entas_2484 (iacR)	MarR family regulatory protein			−8.48	4.96E−09			−9.14	6.10E−09
Entas_2485	4-Hydroxyphenylacetate transporter	2.13	1.24E−09	5.36	5.07E−14			3.16	3.53E−11
Entas_2486	Hypothetical protein			2.78	7.09E−12			2.55	1.27E−10
Entas_2662	Hypothetical protein	1.00	1.93E−03	1.01	2.36E−03				
Entas_2754	Carboxylate/amino acid/amine transporter	1.57	1.88E−07			1.17	2.30E−05		
Entas_2838	Hypothetical protein			1.23	1.84E−02				
Entas_3211	Short-chain dehydrogenase/reductase			1.09	2.76E−02				
Entas_3302	Major facilitator superfamily symporter	1.92	8.37E−05			1.88	2.48E−04		
Entas_3316	PepSY-associated TM helix domain-containing protein			−1.55	2.81E−02				
Entas_3348	Type 1 secretion target domain-containing protein	−1.63	1.81E−05						
Entas_3349	TolC family type I secretion outer membrane	−1.55	1.46E−04						
Entas_3350	Type I secretion system ATPase	−1.22	2.42E−04						
Entas_3351	HlyD family type I secretion membrane fusion	−1.38	1.05E−05						
Entas_3359	Pili assembly chaperone			1.35	1.76E−02				
Entas_3734	Major facilitator superfamily protein							1.09	2.30E−03
Entas_3754	Methyl-accepting chemotaxis sensory transducer	1.24	1.75E−05					−1.03	1.23E−04
Entas_3964	Phage head-tail adaptor			1.12	1.66E−02				
Entas_3982	TetR family transcriptional regulator			2.04	5.95E−03				
Entas_3987	ABC transporter, periplasmic subunit	−1.19	1.81E−05						
Entas_3988	Amino acid ABC transporter inner membrane	−1.13	7.36E−05						
Entas_3989	Amino acid ABC transporter inner membrane	−1.07	6.90E−05						
Entas_4058	Malonate decarboxylase subunit beta	1.24	2.20E−05						
Entas_4059	Malonate decarboxylase acyl carrier protein	1.33	3.65E−03						
Entas_4060	Triphosphoribosyl-dephospho-CoA synthase	1.58	3.55E−05						
Entas_4061	Malonate decarboxylase subunit alpha	1.34	3.59E−06						
Entas_4076	Nitrite reductase [NAD(P)H], small subunit					−1.34	2.99E−02		
Entas_4256	Homoserine/threonine efflux pump	1.04	8.68E−06						
Entas_4332	Oligogalacturonate-specific porin			1.28	3.80E−02				
Entas_4489	Hypothetical protein	1.87	1.20E−07			1.89	6.88E−07		
Entas_4490	Hypothetical protein	1.86	2.03E−08			1.84	2.28E−07		
Entas_4528	Hypothetical protein			1.41	2.23E−02				
Entas_4589	LuxR family regulatory protein			1.41	5.42E−03				
Entas_4676	Tail X family protein							1.29	1.56E−02
Entas_R0064	5S rRNA			2.92	9.86E−03				
Entas_R0084	5S rRNA			2.40	1.74E−02				
Entas_R0090	5S rRNA			2.34	4.01E−02				
Entas_R0101	5S rRNA			2.65	4.84E−02				

[a]Differentially expressed genes have an LFC value smaller than −1 or greater than 1, with an adjusted P value of <0.05. For these genes, LFCs and corresponding P values are shown for four pairwise comparison. A blank entry indicates that the gene was not differentially expressed in that comparison. Gray shading reveals which genes are next to each other on the LF7 chromosome.
[b]wt, wild-type *E. soli* LF7.
[c]mut, Δ*iacR* deletion mutant.

_2662, _4489, and _4490) (Table 1). The seven genes that appeared to be significantly repressed by IAA in wild-type *E. soli* LF7 were found in two clusters on the LF7 chromosome. The first set of genes (Entas_3348-3351; LFC, −1.2 to −1.6) resembles the *lapABCE* system of *Pseudomonas fluorescens*, in which the *lapEBC*-encoded ABC transporter participates in the secretion of LapA, a large protein required for biofilm formation, more specifically, for irreversible surface attachment (9). The second set of IAA-repressed genes (Entas_3987-3989, LFC = −1.1 to −1.2) is annotated to code for components of a general amino acid ABC transport system.

To confirm the notion that *iacR* is a repressor of *iac* gene expression, we compared the RNA-Seq-based transcriptional profile of the *E. soli* LF7 *iacR* deletion mutant (mut) to that of the wild-type *E. soli* LF7 (wt) in the absence of IAA. In this mut−IAA versus wt−IAA comparison, we identified 48 differentially expressed genes: 45 for which
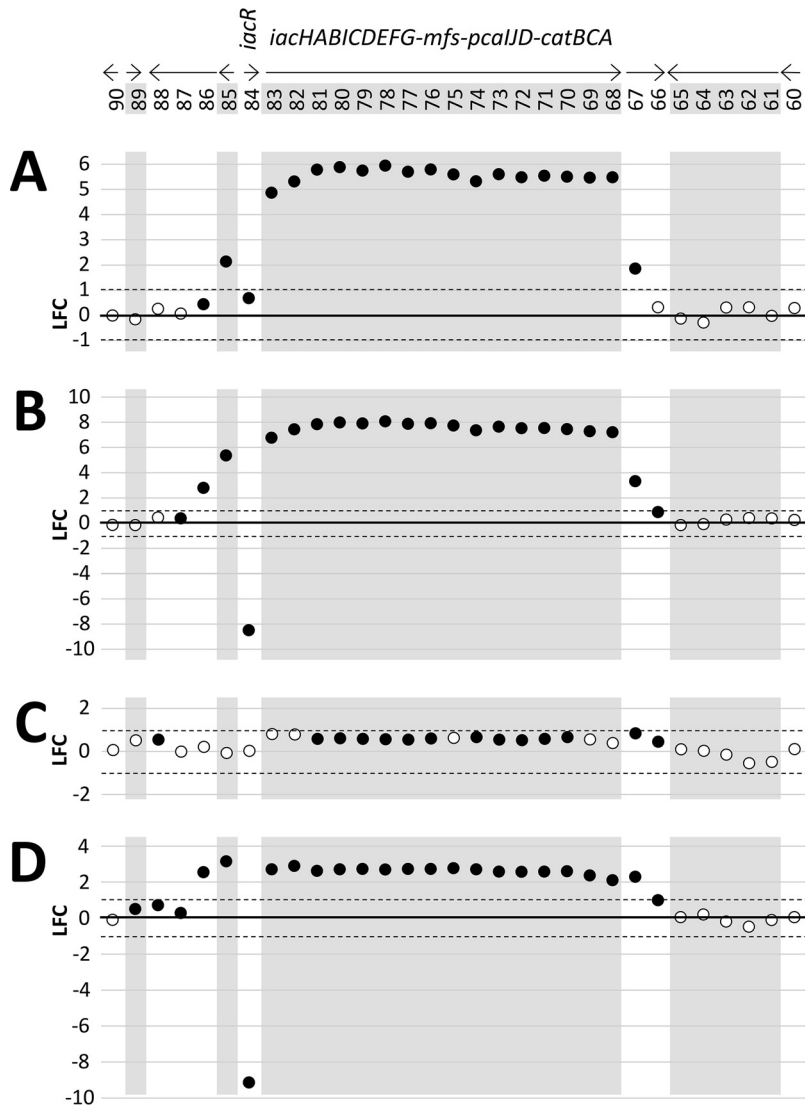
FIG 3 Relative differences in the transcript levels of genes within or near the *iac* gene cluster of succinate-grown *E. soli* LF7 wild-type (wt) and its Δ*iacR* derivative (mut), exposed (+) or not exposed (−) to IAA. Shown are $\log_2$-fold changes (LFC; see the text) for the following comparisons: (A) wt+IAA versus wt−IAA, (B) mut−IAA versus wt−IAA, (C) mut+IAA versus mut−IAA, and (D) mut+IAA versus wt+IAA. Genes are identified by the last two digits of their Entas_24xx locus tag number (see Fig. 1). Filled symbols represent genes for which the adjusted *P* values were <0.05. Dashed lines mark LFC = 1 and LFC = −1 (i.e., 2-fold higher or lower transcript levels, respectively).

transcript levels were higher in the *iacR* mutant than in the wild type, and 3 for which levels were lower (Table 1). The gene with the lowest LFC was *iacR*, as would be expected, given that this gene had been deleted in the Δ*iacR* mutant. Among the 45 induced genes in the mutant, the 18 highest LFC values were observed for the very same genes that were most responsive to IAA in the wild-type strain, namely, *iacHABICDEFG-mfs-pcaIJD-catBCA*, Entas_2485 (upstream of *iacR*), and Entas_2467 (immediately downstream of *catA*) (Fig. 3B). These 18 genes, together with Entas_2662 (hypothetical protein), were the only genes that were (i) induced by IAA in the wild type and (ii) upregulated in the *iacR* deletion mutant. This result is wholly consistent with the proposed role of the *iacR* gene product as a repressor of *iac* gene expression in the absence of IAA and with a mechanism of IAA-induced derepression of *iacHABICDEFG-mfs-pcaIJD-catBCA*, Entas_2485, Entas_2467, and Entas_2662.

The mut+IAA versus mut−IAA comparison showed that in the Δ*iacR* mutant, none of the genes in or near the *iacHABICDEFG-mfs-pcaIJD-catBCA* cluster were differentially
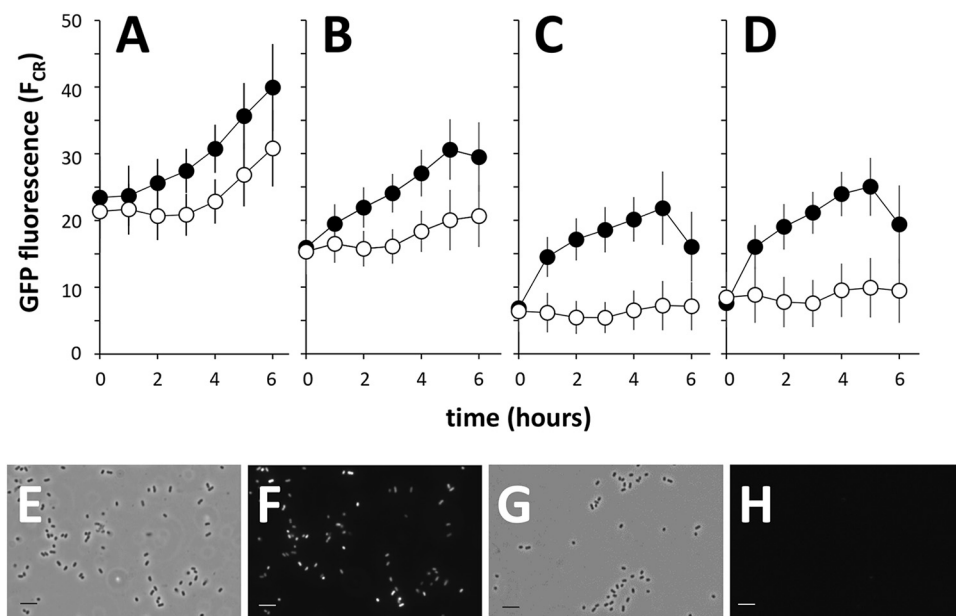
FIG 4 IAA-induced GFP fluorescence in *E. soli* LF7 cells carrying the *iacH* promoter region (P$_{iacH}$) fused to the promoterless *gfp* gene variants tagless (A), ASV (B), AAV (C), or LVA (D). Shown as a function of time since induction with 200 μM IAA (●) or water (control, ○) are the means and standard deviations of single-cell GFP fluorescence (measured by flow cytometry and expressed as the cube root of FL-1, or F$_{CR}$) in bacterial cultures growing exponentially on M9 with succinate. Fluorescence microscope images of *E. soli* LF7(pP$_{iacH}$-*gfp*[AAV]) cells growing exponentially in M9 liquid medium containing 5 mM IAA (E, F) or 12.55 mM succinate (G, H). Shown are representative phase contrast (E, G) or GFP channel (F, H) images. Bars, 5 μm.

expressed in response to IAA (Fig. 3C). This suggests that in the Δ*iacR* mutant, the derepression of these genes is maximal. Only 10 genes responded to IAA in the Δ*iacR* mutant (Table 1). Among the eight that were induced by IAA, six (Entas_0990, _2124, _2754, _3302, _4489, and _4490) were also induced by IAA in the wild type, suggesting that their response to IAA might be *iacR* independent and not related to IAA degradation.

By comparing the transcriptional profiles of the Δ*iacR* mutant to those of the wild-type strain under identical conditions of IAA exposure (i.e., mut+IAA versus wt+IAA), we found 43 genes differentially expressed (Table 1): 13 that showed lower transcript levels in the mutant than in the wild type (including, as expected, *iacR* itself) and 30 that showed higher levels (Table 1). Among the latter were all 16 genes in the *iacHABICDEFG-mfs-pcaIJD-catBCA* cluster, as well as Entas_2467 (fatty acid desaturase), Entas_2485 (4-hydroxyphenylacetate transporter), and Entas_2486 (hypothetical protein) (Fig. 3D). This observation suggests that the derepression of these genes by 200 μM IAA in wild-type LF7 was less than what is achievable by the deletion of *iacR*. The other genes that showed higher expression in the Δ*iacR* mutant than in the wild type in the presence of IAA included Entas_1713-1717 (LFC, 1.1 to 1.3; conversion of arginine to glutamate) and Entas_0525 (LFC = 2.38, annotated to code for carbon starvation protein CstA). The genes that were expressed at lower levels in the Δ*iacR* mutant than in the wild-type strain in the presence of IAA included genes coding for a maltose uptake system (Entas_0262-0264) and carbamoyltransferases or -synthases (Entas_0470-0471, _0478, and _0640).

Identification and characterization of the *iac* promoter/operator region. We focused on the *iacR-iacH* intergenic region as the most likely to harbor the promoter(s) that drives the expression of the *iac* genes, as well as the putative operator(s) that is targeted by the IacR repressor. Cloned upstream of a promoterless *gfp* gene, a 480-bp *iacR-iacH* intergenic fragment (designated P$_{iacH}$) resulted in IAA-inducible expression of green fluorescence in host *E. soli* LF7 (Fig. 4). The relative difference in green fluores-
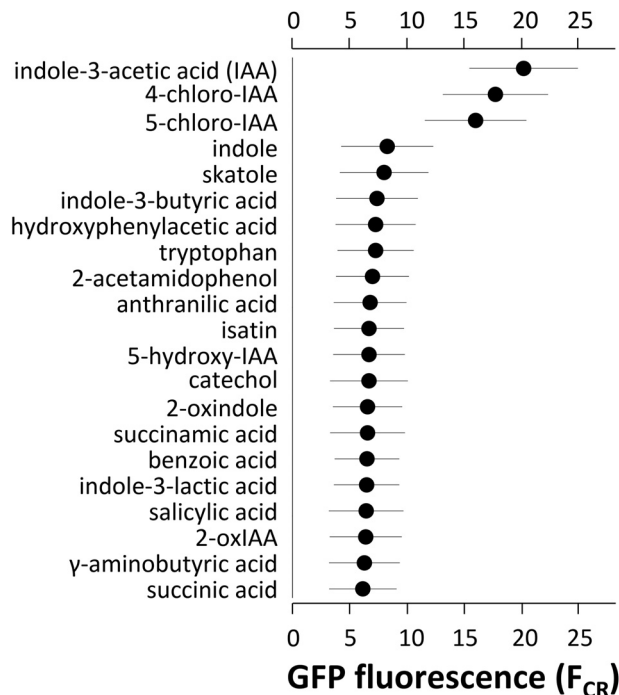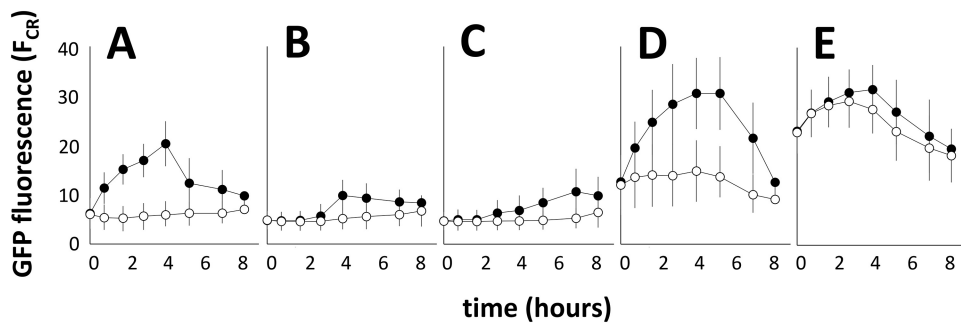
FIG 5 Means and standard deviations of single-cell GFP fluorescence of *E. soli* LF7(pP$_{iacH}$-*gfp*[AAV]) growing in M9 liquid medium with succinate and exposed for 4 to 5 h to 200 μM IAA or one of the other compounds listed, before analysis of single-cell GFP fluorescence by flow cytometry. F$_{CR}$, cube root of the mean of 30,000 cells registered by the FL-1 channel output in flow cytometry.

cence between induced and uninduced cells varied depending on the variant of *gfp* that was used, i.e., *gfp*[tagless] (Fig. 4A), *gfp*[ASV] (Fig. 4B), *gfp*[AAV] (Fig. 4C), or *gfp*[LVA] (Fig. 4D). These variants code for green fluorescent proteins with different half-lives (10). The highest induced-to-uninduced GFP ratio was observed with *gfp*[AAV] (Fig. 4C). Figure 4E to H shows representative images of *E. soli* LF7 cells carrying a P$_{iacH}$-*gfp*[AAV] fusion during growth on IAA or succinate: only during growth on IAA did the cells accumulate green fluorescence.

Inducer specificity and catabolite repression. Cultures of *E. soli* LF7(pP$_{iacH}$-*gfp*[AAV]) were grown on succinate and spiked with various compounds at a concentration of 200 μM to test their ability to induce P$_{iacH}$. The tested compounds were skatole (3-methylindole), 2-oxindole-3-acetic acid, isatin, indole-3-lactic acid, anthranilate, acetamidophenol, 5-hydroxyindoleacetic acid, catechol, indolebutyric acid, salicylate, succinamic acid, tryptophan, benzoate, gamma-aminobutyric acid, hydroxyphenylacetic acid, indole, oxindole, succinate, 4-chloro-indoleacetic acid, 5-chloro-indoleacetic acid, and IAA. Of these, only IAA and its two chlorinated derivatives (4-chloro-IAA and 5-chloro-IAA) were able to induce fluorescence (Fig. 5), suggesting a high specificity for *iac* gene induction. We also tested the ability of *E. soli* LF7(pP$_{iacH}$-*gfp*[AAV]) to respond to 200 μM IAA while growing on carbon sources other than succinate. Compared to succinate (Fig. 6A), both glucose (Fig. 6B) and fructose (Fig. 6C) repressed IAA-induced GFP expression, while on benzoate (Fig. 6D), gene expression was elevated even in the absence of IAA but still inducible with IAA. The highest levels of fluorescence were found with cells growing on IAA (Fig. 6E).

Dose response of *iac* gene expression. To determine the sensitivity of the *iacH* promoter to IAA, we exposed cultures of *E. soli* LF7(pP$_{iacH}$-*gfp*[AAV]) to IAA concentrations ranging from 0 to 1 mM. This experiment revealed a quasi-dose-dependent response to IAA, i.e., no response to IAA in the 0 to 0.36 μM range, a transient accumulation of GFP with 1.6 to 8 μM IAA, and a maximal response at concentrations of 40 μM and higher (Fig. 7A). At concentrations of 1.6 μM or greater, an increase in

FIG 6 Mean GFP fluorescence (and standard deviation) in single cells of *E. soli* LF7(pP*iacH*-*gfp*[AAV]) growing exponentially on 12.55 mM succinate (A), 8.33 mM glucose (B), 8.33 mM fructose (C), 7.14 mM benzoate (D), or 5 mM IAA (E), and spiked at t = 0 with 200 μM IAA (●) or water control (○).

fluorescence was already measurable at the very first sampling point (20 to 25 min after the IAA spike), suggesting a rapid response of P*iacH* to IAA.

We suspected that the transient expression of GFP in IAA-exposed cultures of *E. soli* LF7(pP*iacH*-*gfp*[AAV]) at 1.6 and 8 μM (Fig. 7A) was due to IAA being consumed by the bacteria. To test this hypothesis, we transformed the *iacA* deletion mutant *E. soli* LF7 Δ*iacA*::*cat* (unable to grow on IAA) with the plasmid pP*iacH*-*gfp*[AAV] and measured GFP accumulation in response to IAA. Consistent with our hypothesis, this strain did not show transient expression at low IAA concentrations (Fig. 7B). Instead, GFP reached more or less steady-state levels approximately 2 h after the IAA spike. From these levels, we constructed a dose-response curve for IAA (Fig. 7C), showing a half-maximal response at 3.4 μM IAA and a dose-responsive range between 1 and 20 μM. The results from this experiment also would suggest that IAA, as opposed to an IAA degradation pathway intermediate, is the inducer of *iac* gene expression, assuming that IacA catalyzes the first enzymatic step in the IAA degradation pathway.

Expression of P*iacH*-*gfp* in a Δ*iacR* background. We used the pP*iacH*-*gfp*[AAV] construct to confirm the role of *iacR* as a repressor of *iac* gene expression. For this, we transformed an *iacR* deletion mutant *E. soli* LF7 Δ*iacR*::*cat* with the pP*iacH*-*gfp*[AAV] construct or with an *iacR*-complemented derivative of pP*iacH*-*gfp*[AAV], i.e., p*iacR*-P*iacH*-*gfp*[AAV]. The latter construct harbors a complete *iacR* gene, including its native
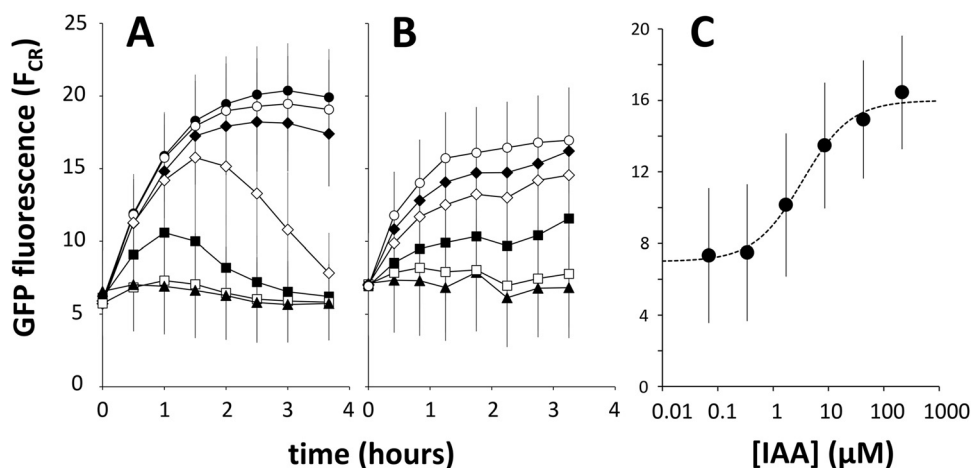
FIG 7 Accumulation of GFP fluorescence in *E. soli* LF7(pP*iacH*-*gfp*[AAV]) cells (A) or in *E. soli* LF7 Δ*iacA*::*cat*(pP*iacH*-*gfp*[AAV]) cells (B) in response to a range of IAA concentrations. Cells were growing exponentially in M9 medium supplemented with 12.55 mM succinate when they were exposed to IAA at time t = 0. IAA concentrations were as follows: ●, 1 mM; ○, 200 μM; ◆, 40 μM; ◇ 8 μM; ■, 1.6 μM; □, 0.32 μM; ▲, no IAA. (C) IAA dose-response curve for *E. soli* LF7 Δ*iacA*::*cat*(pP*iacH*-*gfp*[AAV]) cells. Shown are the GFP fluorescence averages over the time period of 1.25 to 2.75 h after IAA exposure, as a function of IAA concentration. The stippled line represents the best fit of a Hill equation with a coefficient of 1 and a half-maximal GFP fluorescence at 3.4 μM IAA.
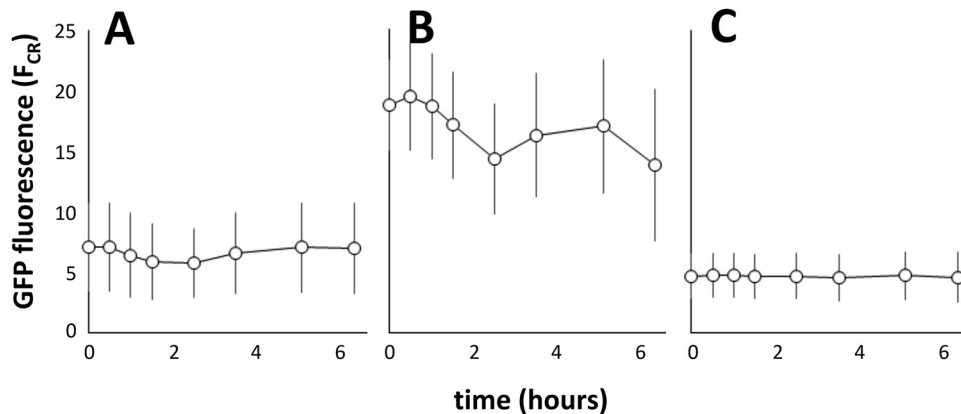
FIG 8 Single-cell GFP fluorescence of *E. soli* LF7(pP$_{iacH}$-*gfp*[AAV]) (A), *E. soli* LF7 Δ*iacR::cat*(pP$_{iacH}$-*gfp*[AAV]) (B), and *E. soli* LF7 Δ*iacR::cat*(p*iacR*-P$_{iacH}$-*gfp*[AAV]) (C) as a function of time. Cells were growing on M9 plus 12.5 mM succinate.

promoter, upstream of the *iacR-iacH* intergenic region. In the absence of IAA, GFP fluorescence in succinate-grown *E. soli* LF7(pP$_{iacH}$-*gfp*[AAV]) was low, as before (Fig. 8A). Under the same conditions, GFP fluorescence in *E. soli* Δ*iacR::cat*(pP$_{iacH}$-*gfp*[AAV]) was elevated to levels that were much higher (Fig. 8B). This result is consistent with the RNA-Seq data which showed that *iacR* is a repressor of expression from the *iacH* promoter. Complementation with *iacR* abolished the constitutive expression of P$_{iacH}$ in *E. soli* LF7 Δ*iacR::cat* (Fig. 8C).

Identification of a putative *iac* promoter/operator region. To identify the location of possible promoter and operator regions upstream of *iacH*, we generated 5′ or 3′ sequential deletions of the 480-bp *iacR-iacH* intergenic space and fused these to *gfp*[AAV] for testing in wild-type *E. soli* LF7. The results of this analysis are shown in Fig. 9. Deletions of 388, 289, 210, 183, and 165 bp from the 3′ end of the P$_{iacH}$ fragment (i.e., constructs F-R1, F-R2, F-R3, F-R3A, and F-R3B, respectively) resulted in a complete loss of the IAA response, whereas no loss was observed following deletions of 145 (construct F-R4) or 86 (construct F-R5) bp from the 3′ end. This result is compatible with the prediction by PromoterHunter (11) of a −35/−10 promoter sequence (TTGAAT-N$_{16}$-CATGAT) at positions 310 to 337 of the P$_{iacH}$ fragment, as F-R1, F-R2, F-R3, F-R3A, and F-R3B lack this sequence (P1) partially or entirely (Fig. 9). Deletions from the other end of the P$_{iacH}$ fragment gave a more complicated result. IAA responsiveness was lost with 5′ deletions of 376, 315, and 297 bp (constructs F5-R, F4-R, and F3B-R, respectively), but not with a deletion of 270 bp (construct F3A-R). This is consistent with a predicted −35/−10 promoter sequence (GTGAAA-N$_{17}$-TCTAAT) at positions 286 to 314 of the P$_{iacH}$ fragment, as F5-R, F4-R, and F3B-R, but not F3A-R, lack this sequence (P2) partially or entirely (Fig. 9). A deletion of 251 or 169 bp from the 5′ end of P$_{iacH}$ (constructs F3-R or F2-R, respectively) also abolished IAA responsiveness, but not a deletion of 72 bp only (construct F1-R). Together, this would suggest that in the absence of the F1-R2 region of P$_{iacH}$ (labeled Z in Fig. 9), the F2-R3 region (labeled Y in Fig. 9) has a negative effect on promoter activity driven from F3A-R4 (labeled X in Fig. 9). We noted that predicted promoters P1 and P2 overlap with each other and with a DNA sequence that represents an imperfect palindromic sequence (5′-GAAACATTACTTGAAT●TTTCATCTA ATTCTTC-3′) that meets the general criterion of a MarR-type regulator binding site (the bullet represents the symmetry center of the palindrome) (12).

DISCUSSION

The work we describe here establishes *E. soli* LF7 as the fourth bacterial strain for which the possession of an *iac* gene cluster has been experimentally linked to the use of IAA as the sole source of carbon and energy. The three other strains with such a link (i.e., *P. putida* 1290, *A. baumannii* ATCC 19606, and *P. phytofirmans* PsJN) were isolated
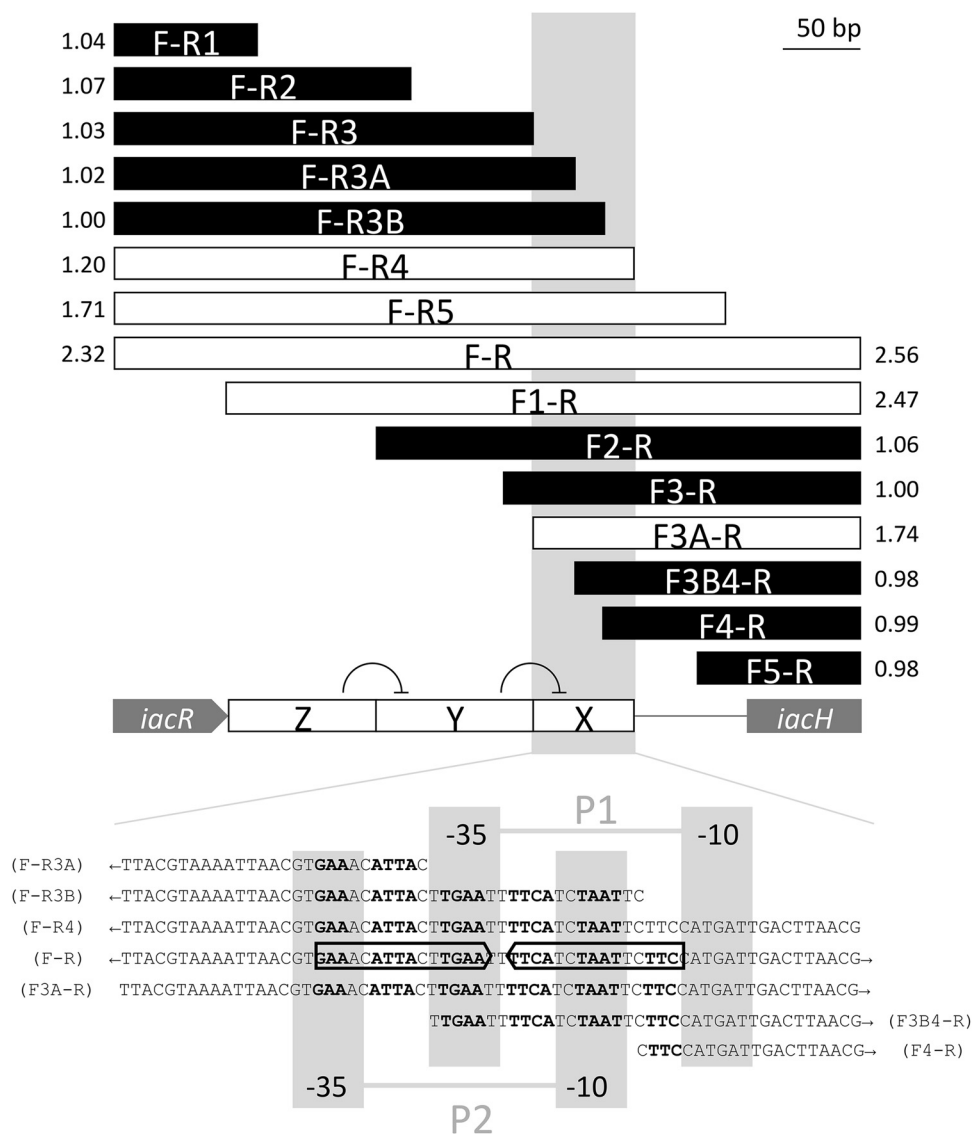
FIG 9 Deletion analysis of the *iacR-iacH* intergenic region to locate putative *iacH* promoters and IacR operator sites. The F-R bar represents the full 480-bp DNA fragment that was amplified from *E. soli* LF7 using primer pair F and R (Table 3) and fused to a promoterless *gfp* gene in pPROBE'-*gfp*[AAV] to test responsiveness to 200 μM IAA in a LF7 wild-type background. All other bars represent subfragments of F-R, using either F or R in combination with another forward or reverse primer (e.g., F-R5 represents an amplicon obtained with primers LF7iacHProm1F and LF7HpromFNDRREV5SalIR, see Table 3). White bars represent fragments that showed IAA inducibility, while black bars represent fragments that did not respond to IAA. The number next to each bar is a measure for inducibility, expressed as the ratio of mean F_{CR} of IAA-exposed cells to the mean F_{CR} of unexposed cells, measured 1 h after IAA exposure. The boxed gray area (also marked as region X on the *iacR-iacH* intergenic region) represents a sequence within F-R that is minimally required for transcriptional response to IAA. Within this sequence (shown at the bottom of the figure), we identified two possible −35/−10 promoters (P1, TTGAAT/CATGAT; and P2, GTGAAA/TCTAAT) as well as an imperfect 16-bp inverted repeat (5′-GAAnnATTAnnTGAAnnTTCAnnTAATnnTTC-3′) overlapping both promoters and possibly representing an IacR operator site. The results of the deletion analysis are consistent with a model where the presence of sequence Z on the *iacR-iacH* intergenic region is required to reverse the negative effect of sequence Y on the IacR-regulated expression of *iacH* from sequence X (see the text for more details on this proposed model).

from plants (3, 13) or urine (14). Plants and urine both contain IAA in quantities that are sufficiently high (15, 16) to justify the maintenance of *iac* genes in support of bacterial growth at the expense of IAA. *E. soli* LF7 was isolated from a Peruvian soil for which IAA measurements, insofar as we know, are not available (8). While IAA levels are generally low in soils (17), concentrations as high as 210 μg/kg have been reported for some organic soils (18), which (assuming a 10% to 60% soil water content) translates into an

IAA concentration range of 2 to 12 μM. It is worth noting that this estimate overlaps with the range of IAA concentrations that, in our experiments, induced *iac* gene expression in *E. soli* LF7 (Fig. 7). We consider this to be at least consistent with the possibility that the *iac* genes contribute to the fitness of *E. soli* LF7, and other *iac*-carrying bacteria, in certain soil environments. The most likely sources of soil IAA are plants and microorganisms, both of which are known to produce IAA and use it as a signal molecule (19). The ability to destroy IAA bestows upon *E. soli* LF7 the potential to interfere with this signaling, especially as it pertains to the root-associated micro-organisms that promote plant growth or suppress the plant innate immunity response by the production of IAA (19). The presence and activity of *iac*-carrying bacteria such as *E. soli* LF7 at the root-soil interface could thus have a significant impact on plant-microbe interactions.

Our study is not the first to generate a genome-wide transcriptional profile of a bacterial response to IAA (20–23). However, we are not aware of a study that did so for an *iac*-carrying bacterium or used RNA-Seq (instead of microarrays). In *E. coli* MG1655 (20) and *Bradyrhizobium japonicum* USDA 110 (23), IAA elicits a generalized stress response; more specifically, it induces phenotypes that increase survival when bacteria are challenged with cold, heat, osmotic, or oxidative shock. The exposure to IAA also stimulated exopolysaccharide production and biofilm formation (20, 23). In *Azospirillum brasilense* Sp245 (22) and *Agrobacterium tumefaciens* C58 (21), IAA elicited a more specific response by impacting the expression of genes that are known to be important for the interaction of these bacteria with their plant host. For example, IAA induced the expression of genes coding for a type VI secretion system (T6SS) in *A. brasilense* and repressed the expression of the *vir* regulon in *A. tumefaciens*. The response to IAA of the bacterium under study here, *E. soli* LF7, is best characterized as specific rather than general: only 44 of 4,582 (<1%) genes were differentially expressed in response to IAA, and of those, 18 were genes in or near the *iac* cluster (including *pca* and *cat* genes) involved in IAA/catechol catabolism. This suggests a response of LF7 to IAA that is highly specific to IAA as a source of carbon and energy. This response includes the activation of Entas_2474 (*mfs*), for which the most similar orthologs in the genome of *P. phytofirmans* PsJN are *iacT1* (Bphyt_2159) and *iacT2* (Bphyt_6111), implemented in the transport of the IAA pathway intermediate diOxIAA (7). The role of Entas_2474 in the transport of IAA(-like compounds) remains untested for LF7, but its coexpression with *iac* genes make it a prime candidate for such a role, together with other predicted transporter genes that were induced in LF7 upon exposure to IAA (i.e., Entas_0990, _1586, _2485, and _3302).

We present several lines of experimental evidence (Fig. 3 and 8) that confirm a role of the *iacR* gene product as a repressor of *iac* gene expression in *E. soli* LF7 in the absence of IAA, as has been previously reported for *A. baumannii* ATCC 19606 (6). MarR-type proteins typically bind to 16- to 20-bp inverted repeats (12). We identified upstream of the first gene in the *iac* cluster of LF7 (i.e., *iacH*) a potential binding site for IacR (Fig. 9). This sequence (5′-GAAAC<u>ATTA</u>C<u>TTG</u>AA<u>TTTT</u>CA<u>TC</u>T<u>AATT</u>C<u>TTC</u>-3′) overlaps with two putative $-35/-10$ promoters for *iacH* expression (Fig. 9). Interestingly, the center portion of this DNA sequence shows significant homology to the MarR DNA-binding site II of *E. coli*, which is 5′-<u>ATTAC</u>TT<u>G</u>ccagggC<u>A</u>a<u>CTAAT</u>-3′ (identical nucleotides capitalized). The binding of IacR at this location sterically prevents RNA polymerase from interacting with the putative *iacH* promoter(s). A deletion analysis of the LF7 *iacR-iacH* intergenic region (Fig. 9) suggests, however, that the regulation of *iac* gene expression in this bacterium involves more than just IacR and RNA polymerase. The analysis is consistent with a model that divides the *iacR-iacH* intergenic region into three functional sections, X, Y, and Z (Fig. 9), where X encompasses the *iacH* $-35/-10$ promoter(s) and IacR-binding site and is sufficient for inducible expression of *iacH*, Y represents a DNA sequence that silences *iacH* gene expression from section X, and Z is required to suppress the activity of Y. In the context of this proposed model for P_{iacH} expression, it is interesting to note the placement of a large, imperfect inverted repeat across sections Z and Y, where one part of the repeat is located in section Z (5′-<u>TAA</u>

nGCAAAAAAnnCGAA-n$_{63}$-AACCGCnGnTGCAA-3') and separated by 4 nucleotides (5'-GTGA-3') from the other repeat in section Y (5'-TTGCAnCnGCGGTT-n$_9$-TTCGnnTTT TTTGCnTTA-3'). Interestingly, immediately downstream of the repeat in section Y is a stretch of DNA (5'-TTTTCATC-3') that is directly repeated in section X and overlaps with both of the predicted −35/−10 promoters as well as with the proposed lacR binding site. This configuration might point to the involvement of a secondary DNA structure to stabilize transcription from the *iacH* promoter.

It is worth remarking that the *E. soli* LF7(pP$_{iacH}$-*gfp*[AAV]) strain that we generated and used in this study has several characteristics that make it a suitable bacterial bioreporter (24) for IAA. Because its output is GFP fluorescence, the exposure to IAA can be assessed at the resolution of single cells (Fig. 4E to H), which permits the interrogation of environments where IAA availability is suspected to be spatially heterogeneous, such as plant surfaces or tissues (25). The response of *E. soli* LF7(pP$_{iacH}$-*gfp*[AAV]) to IAA is quick and sensitive to a range of concentrations that are biologically relevant, not only in soils as already explained above, but also in plants (16, 21) and animal urine (15). Also, the response of *E. soli* LF7(pP$_{iacH}$-*gfp*[AAV]) appears to be specific to IAA and its chlorinated derivatives (Fig. 5), which would limit false-positive feedback from the bioreporter. A notable exception to the specificity of *E. soli* LF7(pP$_{iacH}$-*gfp*[AAV]) is benzoate, which did not induce *iac* expression when added at 200 μM to a culture growing on succinate (Fig. 5) but did so during growth on 7.14 mM benzoate as the sole source of carbon and energy (Fig. 6D). For comparison, the *iac* genes in *P. phytofirmans* PsJN were not induced during the growth of PsJN on benzoate (7). In the LF7 genome, there appears to be no additional set of *catBCA* and *pcalJD* genes beside the one (Entas_2468-2473) that lies immediately downstream of the *iac* genes. Since these genes code for shuttling catechol into central metabolism, and since catechol typically is the end product of benzoate degradation pathways (26), perhaps the induction of *iac* genes during growth on benzoate may be interpreted to mean that the *cat* and *pca* genes are transcriptionally coupled to the *iac* genes in LF7. In other words, to utilize catechol produced from benzoate, the expression of *cat* and *pca* is needed, which would require the expression of the *iac* genes if *cat* and *pca* were part of the same operon as the *iac* genes. However, this invites the question of what, during growth on benzoate, is the inducer of *iac* expression, if not IAA. An even more pertinent question is how *E. soli* LF7 is able to grow on benzoate in the first place. The *E. soli* LF7 genome features at least one gene (Entas_2116) that is annotated to code for a benzoate transporter but no genes that are linked to enzymes in known benzoate degradation pathways, such as Bphyt_1591-1594 (*benABCD*) in *P. phytofirmans* PsJN (GenBank accession numbers WP_012432614 to WP_012432617). These benzoate anomalies require an experimental scrutiny that is beyond the scope of the study described here.

The syntenic arrangement of *iac* genes on the LF7 genome and the proximity to and IAA-specific coexpression with *pca* and *cat* genes can be interpreted as an adaptation that enables the efficient and complete degradation of IAA into components of the citric acid cycle for the generation of cellular building blocks and energy. Under this assumption, the *iacHABICDEFG-mfs-pcalJD-catBCA* arrangement as it is found in LF7 would make most sense in environments where IAA is available as a food source and in (relative) abundances that offer its bacterial host a competitive advantage over other bacteria. Interestingly, the exact same gene arrangement can be found on the genomes of other *Enterobacteriaceae*, including *Lelliottia* sp. PFL01 (27), *Leclercia* sp. LSNIH1 and LSNIH3 (28), and *Leclercia adecarboxylata* strain USDA-ARS-USMARC-60222 (29). However, the environments from which these particular strains were isolated are very different, i.e., fermented seafood (27), hospital plumbing (28), and livestock (29), respectively. This confirms that while the possession of *iac* genes is a good predictor of its host being able to grow at the expense of the plant hormone IAA (as shown for *E. soli* LF7 here), it is not prognostic of a plant-environmental origin of the *iac*-carrying bacterial host. An independent case in point for the latter is presented by the *iaa* genes, which were first described in 2012 (30) as underlying the ability of the betaproteobac-

TABLE 2 Strains and plasmids used in this study

Strain or plasmid	Description	Reference or source
Strains		
Enterobacter soli LF7	Can utilize IAA as sole carbon source (this study)	8
Enterobacter soli LF7 Δ*iacA*::*cat*	*E. soli* LF7 derivative; *iacA* replaced with *cat* gene	This study
Enterobacter soli LF7 Δ*iacR*::*cat*	*E. soli* LF7 derivative; *iacR* replaced with *cat* gene	This study
Escherichia coli TOP10	Cloning host	Thermo Fisher Scientific
Escherichia coli MB613	Host of pKD3 harboring *cat* gene	32
Escherichia coli MB616	Host of pKD46	32
Plasmids		
pPROBE'-*gfp*[tagless]	*gfp* expression vector	10
pPROBE'-*gfp*[LVA]	*gfp*[LVA] expression vector	10
pPROBE'-*gfp*[AAV]	*gfp*[AAV] expression vector	10
pPROBE'-*gfp*[ASV]	*gfp*[ASV] expression vector	10
pCR2.1TOPO	PCR amplicon cloning vector	Thermo Fisher Scientific
pP$_{iacH}$-*gfp*[tagless]	P$_{iacH}$ fragment (F-R) fused to *gfp*[tagless]	This study
pP$_{iacH}$-*gfp*[LVA]	P$_{iacH}$ fragment (F-R) fused to *gfp*[LVA]	This study
pP$_{iacH}$-*gfp*[AAV]	P$_{iacH}$ fragment (F-R) fused to *gfp*[AAV]	This study
pP$_{iacH}$-*gfp*[ASV]	P$_{iacH}$ fragment (F-R) fused to *gfp*[ASV]	This study
p*iacR*-P*iacH*-*gfp*[AAV]	*iacR*-P*iacH* fragment fused to *gfp*[AAV]	This study
pP$_{iacH}$-*gfp*[AAV]FNDR1	P$_{iacH}$ subfragment (F1-R) fused to *gfp*[AAV]	This study
pP$_{iacH}$-*gfp*[AAV]FNDR2	P$_{iacH}$ subfragment (F2-R) fused to *gfp*[AAV]	This study
pP$_{iacH}$-*gfp*[AAV]FNDR3	P$_{iacH}$ subfragment (F3-R) fused to *gfp*[AAV]	This study
pP$_{iacH}$-*gfp*[AAV]FNDR3A	P$_{iacH}$ subfragment (F3A-R) fused to *gfp*[AAV]	This study
pP$_{iacH}$-*gfp*[AAV]FNDR3B4	P$_{iacH}$ subfragment (F3B4-R) fused to *gfp*[AAV]	This study
pP$_{iacH}$-*gfp*[AAV]FNDR4	P$_{iacH}$ subfragment (F4-R) fused to *gfp*[AAV]	This study
pP$_{iacH}$-*gfp*[AAV]FNDR5	P$_{iacH}$ subfragment (F5-R) fused to *gfp*[AAV]	This study
pP$_{iacH}$-*gfp*[AAV]FNDR1REV	P$_{iacH}$ subfragment (F-R1) fused to *gfp*[AAV]	This study
pP$_{iacH}$-*gfp*[AAV]FNDR2REV	P$_{iacH}$ subfragment (F-R2) fused to *gfp*[AAV]	This study
pP$_{iacH}$-*gfp*[AAV]FNDR3REV	P$_{iacH}$ subfragment (F-R3) fused to *gfp*[AAV]	This study
pP$_{iacH}$-*gfp*[AAV]FNDR3AREV	P$_{iacH}$ subfragment (F-R3A) fused to *gfp*[AAV]	This study
pP$_{iacH}$-*gfp*[AAV]FNDR3BREV	P$_{iacH}$ subfragment (F-R3B) fused to *gfp*[AAV]	This study
pP$_{iacH}$-*gfp*[AAV]FNDR4REV	P$_{iacH}$ subfragment (F-R4) fused to *gfp*[AAV]	This study
pP$_{iacH}$-*gfp*[AAV]FNDR5REV	P$_{iacH}$ subfragment (F-R5) fused to *gfp*[AAV]	This study

terium *Aromatoleum aromaticum* strain EbN1 to degrade IAA anaerobically, although strain EbN1 was originally isolated from river mud samples with no obvious plant association (31). The discovery of bacterial IAA catabolism in these environments pleads for studies that examine in more detail the genesis and/or accumulation of IAA in nonplant microbial habitats and its exploitation by microorganisms in those habitats.

MATERIALS AND METHODS

Bacterial strains and growth conditions. The bacterial strains used in this study are listed in Table 2. *E. soli* LF7 was obtained as accession number B-59409 from the USDA-ARS Culture Collection (https://nrrl.ncaur.usda.gov). The deletion mutants of LF7 (Δ*iacA* and Δ*iacR*) were generated by the protocol of Datsenko and Wanner (32) using *E. coli* strains MB613 and MB616 (kindly shared by Maria Brandl, USDA-ARS, Albany, CA). For this purpose, primer sets RedLF7iacApKD4F/R and RedLF7iacRpKD4F/R were designed to generate an amplicon that carries the *cat* (chloramphenicol resistance) gene of MB613 flanked on either side with 50-bp sequences immediately upstream and downstream of *iacA* and *iacR*, respectively (Table 3). PCR was done with GoTaq Green master mix (Promega, Madison WI) with the following settings: 95°C for 5 min, 30 cycles of 94°C for 30 s, 59°C for 30 s, and 72°C for 2 min, and then 72°C for 5 min. *E. soli* LF7 was transformed with plasmid pKD46 from MB616 using a Bio-Rad Gene Pulser Xcell (Bio-Rad, Hercules, CA) according to the manufacturer's recommendations. RedLF7iacApKD4F/R and RedLF7iacRpKD4F/R amplicons were digested with NdeI, purified (Qiaquick PCR purification kit; Qiagen), and electroporated into *E. soli* LF7(pKD46). The transformants were screened for growth on LB agar plates containing chloramphenicol and checked by PCR for the loss of *iacA* or *iacR*. The confirmed deletion mutants of *iacA* and *iacR* are referred to as *E. soli* LF7 Δ*iacA*::*cat* and *E. soli* LF7 Δ*iacR*::*cat*, respectively.

In a typical growth experiment, LF7 or one of its derivatives (LF7 Δ*iacA*::*cat*, LF7 Δ*iacR*::*cat*, or LF7 carrying an *iac* plasmid construct, see below) was grown overnight at 28°C, with shaking at 250 rpm, in lysogeny broth (LB) (33) supplemented with antibiotics as appropriate. After centrifugation of overnight cultures at 2,500 × *g* for 5 min, the bacterial pellets were resuspended in sterile phosphate-buffered saline (PBS), centrifuged and resuspended again, and diluted 100-fold in M9 minimal medium (33) containing 12.5 mM succinate (or another carbon source), 0.2% Casamino Acids, and 6.58 μM FeSO$_4$ and supplemented with antibiotics as appropriate. M9 cultures were incubated at 28°C, with shaking at 250 rpm. For growth on solid medium, agar was added to M9 or LB at a concentration of 1.5%. Antibiotics

TABLE 3 Primers used in this study

Primer	Sequence (5′→3′)
LF7MarRF2	GGGGCCAGCGTTCCGTTCTGG
LF7iacHProm1F (F)	GGAATGACCCGTAATCAGGTCG
LF7HpromFNDR1F (F1)	TAAGGCAAAAAAACCGAATG
LF7HpromFNDR2F (F2)	GATTGCAGCGGCGGTTCTTGCC
LF7HpromFNDR3F (F3)	GGTTAATAAAATGTTGCTG
LF7HpromFNDR3AF (F3A)	TTACGTAAAATTAACGTGAAACATTAC
LF7HpromFNDR3B4F (F3B4)	TTGAATTTTCATCTAATTCTTCCATGATTGACTTAACG
LF7HpromFNDR4F (F4)	CTTCCATGATTGACTTAACG
LF7HpromFNDR5F (F5)	GTGATTCAACATTTCTGG
LF7iacHpromSalIR (R)	GTCGACGGCGAAGCGCAGATCGCCTTCG
LF7HpromFNDRREV5SalIR (R5)	GTCGACCCAGAAATGTTGAATCAC
LF7HpromFNDRREV4SalIR (R4)	GTCGACCGTTAAGTCAATCATGGAAG
LF7HpromFNDRREV3BSalIR (R3B)	GTCGACGAATTAGATGAAAATTCAA
LF7HpromFNDRREV3ASalIR (R3A)	GTCGACGTAATGTTTCACGTTAATTTTACGTAA
LF7HpromFNDRREV3SalIR (R3)	GTCGACCAGCAACATTTTATTAACC
LF7HpromFNDRREV2SalIR (R2)	GTCGACGGCAAGAACCGCCGCTGCAATC
LF7HpromFNDRREV1SalIR (R1)	GTCGACCATTCGGTTTTTTTGCCTTA
RedLF7iacRpKD4F	TTCGCAGGGTATAATCGCGTTATCTGCCGCTTTTTTTGGTAAGGAAACGCGTGTAGGCTGGAGCTGCTTC
RedLF7iacRpKD4R	TAAAACTAATTTCTACGCAGGTCACAAATTTGTCATTCGGTTTTTTTGCCATGGGAATTAGCCATGGTCC
RedLF7iacApKD4F	GCGGCCCCGTTCGCCCTCGCGACAGCCGCGGATAACTTTTCGGAGGTCGCGTGTAGGCTGGAGCTGCTTC
RedLF7iacApKD4R	CAAAACAGCACGCGTAAGGTGGTTGACTGGCTCATGTGTTGCTCCTTTCGATGGGAATTAGCCATGGTCC

were added to the following final concentrations: kanamycin, 50 μg · ml^{-1}; ampicillin, 30 μg · ml^{-1}; chloramphenicol, 25 μg · ml^{-1}.

RNA-Seq analysis of *E. soli* LF7 and *E. soli* LF7 Δ*iacR*::*cat* in response to IAA. After 3 h of growth in M9 medium with succinate (see above), three replicate cultures (each) of wild-type *E. soli* LF7 and *E. soli* LF7 Δ*iacR*::*cat* were spiked with 200 μM IAA (Sigma-Aldrich, Bangalore, India), while another three replicate cultures of each strain were spiked with water (control). After 2 h of additional incubation, all 12 cultures (2 strains, with or without IAA, 3 replicates for each) were treated with 3 volumes of bacterial RNAprotect (Qiagen), followed by total RNA isolation using an RNeasy kit (Qiagen) as per the manufacturer's instructions, which included the DNase I treatment. RNA quality and concentration were checked on an Agilent Bioanalyzer prior to submission to the UC Davis Expression Analysis Core Facility for rRNA depletion, cDNA synthesis, library preparation, and sequencing using the HiSEQ4000 SR50 platform. Single-end reads (50 bp) were subjected to adapter trimming using Scythe (https://github.com/vsbuffalo/scythe), followed by base-quality trimming by sickle (https://github.com/najoshi/sickle). Bases with quality of less than 30 were trimmed, and all reads that were less than 30 bp were removed. Reads that passed quality control were queried against the SILVA rRNA database v123.1 (34) to remove rRNA contamination. The remaining reads were aligned to the *E. asburiae* LF7a genome (GenBank accession number NC_015968) using Rockhopper (35). The parameters were set to account for the second-strand sequencing protocol. Raw-counts data for each annotated feature in the genome were generated by Rockhopper. Genes with less than 1 count-per-million in all samples were removed prior to analysis, leaving a total of 4,582 genes. The counts were normalized using the calcNormFactors function from the edgeR package (36). Differential expression analyses were conducted using limma-voom (http://www.genomebiology.com/2014/15/2/R29). We used Softberry's online FGENESB tool (http://www.softberry.com/berry.phtml?topic=index&group=programs&subgroup=gfindb) for bacterial operon and gene prediction.

Construction of *iac* promoter-*gfp* fusion constructs. Using primers LF7iacHProm1F and LF7iacHpromSalIR (Table 3), the intergenic region between *iacR* and *iacH* was amplified as a 480-bp fragment that stretches from 72 bp into the 3′ end of the *iacR* gene to 72 bp beyond the start codon of *iacH*. We refer to this fragment as P$_{iacH}$ or F-R. We also generated a series of 5′ deletion derivatives of P$_{iacH}$ by using primer LF7iacHpromSalIR in combination with so-called FNDR forward primers (Table 3) that targeted the *iacR*-*iacH* intergenic space in different positions and produced increasingly shorter fragments of 409, 312, 230, 211, 184, 166, or 105 bp. Similarly, we used primer LF7iacHProm1F in combination with so-called FNDRREV primers (Table 3) to generate 3′-end deletion derivatives sized 92, 191, 270, 297, 316, 335, or 394 bp. Using primers LF7MarRF2 and LF7iacHpromSalIR (Table 3), we generated an amplicon that encompasses P$_{iacH}$ as well as a full copy of *iacR* and its presumed promoter. PCRs were performed as described above. PCR products were ligated into vector pCR2.1-TOPO-TA (Thermo Fisher Scientific), transformed into *E. coli* TOP10, excised as an EcoRI/SalI fragment (EcoRI located in the vector, SalI located in the reverse primer), and ligated into EcoRI/SalI-digested pPROBE′-*gfp*[tagless], -*gfp*[AAV], -*gfp*[ASV], and/or -*gfp*[LVA] for transformation into *E. coli* TOP10 and subsequently *E. soli* LF7.

Flow cytometry and fluorescence microscopy. Flow cytometry was performed on live *E. soli* LF7 cells harvested from M9 cultures by centrifugation at 10,000 × *g* for 1.5 min at 4°C and resuspended in 1 ml phosphate-buffered saline (33). Settings on the Accuri C6 flow cytometer (BD Biosciences) were as follows: "slow" speed (14 μl/min; core size, 10 μm) with an event threshold of 20,000 FSC (forward scatter), to collect 30,000 events for each sample. Fluorescence data for individual samples was exported

as comma-separated value spreadsheets (Microsoft Excel), and each data point collected in the FL-1 channel (green fluorescence) was cube-root (CR) transformed into an F_{CR} value, representing the GFP content of each individual cell. Microscopy was performed on a Zeiss Axio Imager.M2 (Carl Zeiss MicroImaging Gmbh, Göttingen, Germany) using an EC Plan-Neofluar ×100/1.30 oil objective (Zeiss) and Axiocam MRm camera (Zeiss). Light sources were a halogen 12-V 100-W lamp at 2.7 V for phase contrast imaging and a mercury vapor short-arc lamp (HBO 103W2) at 75% intensity passed through a Zeiss Filter 38 (BP 470/40, FT 495, BP525/50) to visualize GFP fluorescence. Images were captured at a 50-ms exposure time for both phase contrast and GFP channels.

Accession number(s). Supporting RNA-Seq data have been deposited in the Gene Expression Omnibus (GEO) database (https://www.ncbi.nlm.nih.gov/geo/) and are available under accession number GSE114050.

REFERENCES

1. Proctor MH. 1958. Bacterial dissimilation of indoleacetic acid: a new route of breakdown of the indole nucleus. Nature 181:1345. https://doi.org/10.1038/1811345a0.
2. Leveau JHJ, Gerards S. 2008. Discovery of a bacterial gene cluster for catabolism of the plant hormone indole 3-acetic acid. FEMS Microbiol Ecol 65:238–250. https://doi.org/10.1111/j.1574-6941.2008.00436.x.
3. Leveau JHJ, Lindow SE. 2005. Utilization of the plant hormone indole-3-acetic acid for growth by *Pseudomonas putida* strain 1290. Appl Environ Microbiol 71:2365–2371. https://doi.org/10.1128/AEM.71.5.2365-2371.2005.
4. Scott JC, Greenhut IV, Leveau JH. 2013. Functional characterization of the bacterial *iac* genes for degradation of the plant hormone indole-3-acetic acid. J Chem Ecol 39:942–951. https://doi.org/10.1007/s10886-013-0324-x.
5. Lin GH, Chen HP, Huang JH, Liu TT, Lin TK, Wang SJ, Tseng CH, Shu HY. 2012. Identification and characterization of an indigo-producing oxygenase involved in indole 3-acetic acid utilization by *Acinetobacter baumannii*. Antonie Van Leeuwenhoek 101:881–890. https://doi.org/10.1007/s10482-012-9704-4.
6. Shu HY, Lin LC, Lin TK, Chen HP, Yang HH, Peng KC, Lin GH. 2015. Transcriptional regulation of the *iac* locus from *Acinetobacter baumannii* by the phytohormone indole-3-acetic acid. Antonie Van Leeuwenhoek 107:1237–1247. https://doi.org/10.1007/s10482-015-0417-3.
7. Donoso R, Leiva-Novoa P, Zuniga A, Timmermann T, Recabarren-Gajardo G, Gonzalez B. 2017. Biochemical and genetic bases of indole-3-acetic acid (auxin phytohormone) degradation by the plant-growth-promoting rhizobacterium *Paraburkholderia phytofirmans* PsJN. Appl Environ Microbiol 83:e01991-16. https://doi.org/10.1128/AEM.01991-16.
8. Manter DK, Hunter WJ, Vivanco JM. 2011. *Enterobacter soli* sp nov.: a lignin-degrading gamma-proteobacteria isolated from soil. Curr Microbiol 62:1044–1049. https://doi.org/10.1007/s00284-010-9809-9.
9. Hinsa SM, Espinosa-Urgel M, Ramos JL, O'Toole GA. 2003. Transition from reversible to irreversible attachment during biofilm formation by *Pseudomonas fluorescens* WCS365 requires an ABC transporter and a large secreted protein. Mol Microbiol 49:905–918. https://doi.org/10.1046/j.1365-2958.2003.03615.x.
10. Miller WG, Leveau JH, Lindow SE. 2000. Improved *gfp* and *inaZ* broad-host-range promoter-probe vectors. Mol Plant Microbe Interact 13:1243–1250. https://doi.org/10.1094/MPMI.2000.13.11.1243.
11. Klucar L, Stano M, Hajduk M. 2010. phiSITE: database of gene regulation in bacteriophages. Nucleic Acids Res 38:D366–D370. https://doi.org/10.1093/nar/gkp911.
12. Grove A. 2013. MarR family transcription factors. Curr Biol 23:R142–R143. https://doi.org/10.1016/j.cub.2013.01.013.
13. Frommel MI, Nowak J, Lazarovits G. 1991. Growth enhancement and developmental modifications of *in vitro* grown potato (*Solanum tuberosum* spp. *tuberosum*) as affected by a nonfluorescent *Pseudomonas* sp. Plant Physiol 96:928–936. https://doi.org/10.1104/pp.96.3.928.
14. Hugh R, Reese R. 1968. A comparison of 120 strains of *Bacterium anitratum* Schaub and Hauber with the type strain of this species. Int J Syst Evol Microbiol 18:207–229. https://doi.org/10.1099/00207713-18-3-207.
15. Anderson GM, Purdy WC. 1979. Liquid chromatographic-fluorometric system for the determination of indoles in physiological samples. Anal Chem 51:283–286. https://doi.org/10.1021/ac50038a030.
16. Bandurski RS, Schulze A. 1977. Concentration of indole-3-acetic acid and its derivatives in plants. Plant Physiol 60:211–213. https://doi.org/10.1104/pp.60.2.211.
17. Martens DA, Frankenberger WTJ. 1993. Stability of microbial-produced auxins derived from L-tryptophan added to soil. Soil Sci 155:263–271. https://doi.org/10.1097/00010694-199304000-00005.
18. Szajdak L, Maryganova V. 2007. Occurrence of IAA auxin in some organic soils. Agron Res 5:175–187.
19. Spaepen S, Vanderleyden J. 2011. Auxin and plant-microbe interactions. Cold Spring Harb Perspect Biol 3:a001438. https://doi.org/10.1101/cshperspect.a001438.
20. Bianco C, Imperlini E, Calogero R, Senatore B, Amoresano A, Carpentieri A, Pucci P, Defez R. 2006. Indole-3-acetic acid improves *Escherichia coli*'s defences to stress. Arch Microbiol 185:373–382. https://doi.org/10.1007/s00203-006-0103-y.
21. Yuan ZC, Haudecoeur E, Faure D, Kerr KF, Nester EW. 2008. Comparative transcriptome analysis of *Agrobacterium tumefaciens* in response to plant signal salicylic acid, indole-3-acetic acid and gamma-amino butyric acid reveals signalling cross-talk and *Agrobacterium*–plant co-evolution. Cell Microbiol 10:2339–2354. https://doi.org/10.1111/j.1462-5822.2008.01215.x.
22. Van Puyvelde S, Cloots L, Engelen K, Das F, Marchal K, Vanderleyden J, Spaepen S. 2011. Transcriptome analysis of the rhizosphere bacterium *Azospirillum brasilense* reveals an extensive auxin response. Microb Ecol 61:723–728. https://doi.org/10.1007/s00248-011-9819-6.
23. Donati AJ, Lee HI, Leveau JH, Chang WS. 2013. Effects of indole-3-acetic acid on the transcriptional activities and stress tolerance of *Bradyrhizobium japonicum*. PLoS One 8:e76559. https://doi.org/10.1371/journal.pone.0076559.
24. Leveau JH, Lindow SE. 2002. Bioreporters in microbial ecology. Curr Opin Microbiol 5:259–265. https://doi.org/10.1016/S1369-5274(02)00321-1.
25. Brandl MT, Quinones B, Lindow SE. 2001. Heterogeneous transcription of an indoleacetic acid biosynthetic gene in *Erwinia herbicola* on plant surfaces. Proc Natl Acad Sci U S A 98:3454–3459. https://doi.org/10.1073/pnas.061014498.
26. Pérez-Pantoja D, De la Iglesia R, Pieper DH, Gonzalez B. 2008. Metabolic reconstruction of aromatic compounds degradation from the genome of the amazing pollutant-degrading bacterium *Cupriavidus necator*

JMP134. FEMS Microbiol Rev 32:736–794. https://doi.org/10.1111/j.1574-6976.2008.00122.x.

27. Yuk KJ, Kim YT, Huh CS, Lee JH. 2018. *Lelliottia jeotgali* sp. nov., isolated from a traditional Korean fermented clam. Int J Syst Evol Microbiol 68:1725–1731. https://doi.org/10.1099/ijsem.0.002737.

28. Weingarten RA, Johnson RC, Conlan S, Ramsburg AM, Dekker JP, Lau AF, Khil P, Odom RT, Deming C, Park M, Thomas PJ, NISC Comparative Sequencing Program, Henderson DK, Palmore TN, Segre JA, Frank KM. 2018. Genomic analysis of hospital plumbing reveals diverse reservoir of bacterial plasmids conferring carbapenem resistance. mBio 9:e02011-17. https://doi.org/10.1128/mBio.02011-17.

29. DeDonder KD, Apley MD, Li M, Gehring R, Harhay DM, Lubbers BV, White BJ, Capik SF, KuKanich B, Riviere JE, Tessman RK. 2016. Pharmacokinetics and pharmacodynamics of gamithromycin in pulmonary epithelial lining fluid in naturally occurring bovine respiratory disease in multisource commingled feedlot cattle. J Vet Pharmacol Ther 39:157–166. https://doi.org/10.1111/jvp.12267.

30. Ebenau-Jehle C, Thomas M, Scharf G, Kockelkorn D, Knapp B, Schuhle K, Heider J, Fuchs G. 2012. Anaerobic metabolism of indoleacetate. J Bacteriol 194:2894–2903. https://doi.org/10.1128/JB.00250-12.

31. Rabus R, Widdel F. 1995. Anaerobic degradation of ethylbenzene and other aromatic hydrocarbons by new denitrifying bacteria. Arch Microbiol 163:96–103. https://doi.org/10.1007/BF00381782.

32. Datsenko KA, Wanner BL. 2000. One-step inactivation of chromosomal genes in *Escherichia coli* K-12 using PCR products. Proc Natl Acad Sci U S A 97:6640–6645. https://doi.org/10.1073/pnas.120163297.

33. Sambrook J, Russell DW. 2001. Molecular cloning: a laboratory manual, 3rd ed. Cold Spring Harbor Laboratory Press, Cold Spring Harbor, NY.

34. Quast C, Pruesse E, Yilmaz P, Gerken J, Schweer T, Yarza P, Peplies J, Glockner FO. 2013. The SILVA ribosomal RNA gene database project: improved data processing and web-based tools. Nucleic Acids Res 41:D590–D596. https://doi.org/10.1093/nar/gks1219.

35. McClure R, Balasubramanian D, Sun Y, Bobrovskyy M, Sumby P, Genco CA, Vanderpool CK, Tjaden B. 2013. Computational analysis of bacterial RNA-Seq data. Nucleic Acids Res 41:e140. https://doi.org/10.1093/nar/gkt444.

36. Robinson MD, McCarthy DJ, Smyth GK. 2010. edgeR: a Bioconductor package for differential expression analysis of digital gene expression data. Bioinformatics 26:139–140. https://doi.org/10.1093/bioinformatics/btp616.